This article has been accepted for inclusion in a future issue of this journal. Content is final as presented, with the exception of pagination.

Aridity Thresholds Determine the Relationships Between Ecosystem Functioning and Remotely Sensed Indicators Across Patagonia

Yanchuang Zhao, Emilio Guirado, Juan J. Gaitán, and Fernando T. Maestre

Abstract—**Emerging evidence suggests that ecosystem responses to increases in atmospheric aridity, a hallmark of climate change, exhibit multiple thresholds across global drylands. However, it is not clear whether aridity thresholds exist in the relationships between ecosystem functions and remotely sensed indicators (RSIs). Assessing this is important because these empirical relationships underpin the statistical models commonly used to estimate ecosystem functioning across large spatial scales, which typically uses data from RSI. We evaluated how the relationships between nutrient cycling index (NCI; a proxy of ecosystem functioning) measured *in situ* and RSI [albedo and normalized difference vegetation index (NDVI)] change along with a wide aridity (1 – [precipitation/potential evapotranspiration]) gradient in Patagonia (Argentina). For doing so, we used field-based NCI data from 235 ecosystems that were surveyed twice (2008–2013 and 2014–2018). Three aridity thresholds were identified when evaluating the RSI–NCI relationships. The first threshold was found around aridity values ranging from 0.44 to 0.60, while the second and third were concentrated around aridity values of 0.69 and 0.82, respectively. These results indicate that RSI–NCI relationships changed drastically along aridity gradients, and these thresholds should be considered when evaluating ecosystem functions using RSI. In addition, we also found that the relationships between NCI and albedos were not significant around aridity values of 0.82. These results were consistent across sampling dates. Our findings imply that empirical models of the RSI–NCI relationship employing only albedos/reflectance as inputs are not reliable under the most arid conditions and can be used to improve the effectiveness of the use of RSI to monitor and predict changes in ecosystem functioning across large environmental gradients in drylands.**

Index Terms—**Aridity threshold, ecosystem function, narrow-band albedo, remote sensing.**

Manuscript received June 23, 2021; revised August 18, 2021; accepted September 11, 2021. This work was supported in part by the Research Foundation of Henan University of Technology under Grant 31401178, in part by the Henan Provincial Science and Technology Research Project under Grant 192102210101, in part by the European Research Council (BIODESERT Project) under ERC Grant Agreement 647038, in part by China Scholarship Council (CSC) under Grant 201909895003, and in part by the PEi040 project of National Institute of Agricultural Technology (INTA) of Argentina and Generalitat Valenciana under Grant CIDEGENT/2018/041. *(Corresponding author: Yanchuang Zhao.)*

Yanchuang Zhao is with the Key Laboratory of Grain Information Processing and Control, Ministry of Education, Henan University of Technology, Zhengzhou 450001, China, and also with the College of Information Science and Engineering, Henan University of Technology, Zhengzhou 450001, China (e-mail: yanchuangzhao@gmail.com).

Emilio Guirado is with the Instituto Multidisciplinar para el Estudio del Medio "Ramón Margalef," Universidad de Alicante, 03690 Alicante, Spain (e-mail: egh828@ual.es).

Juan J. Gaitán is with the Instituto de Suelos, CIRN, INTA, Buenos Aires 01686, Argentina, also with the Departamento de Tecnología, Universidad Nacional de Luján, Luján 6700, Argentina, and also with the National Research Council of Argentina (CONICET), Buenos Aires 01686, Argentina (e-mail: gaitan.juan@inta.gob.ar).

Fernando T. Maestre is with the Instituto Multidisciplinar para el Estudio del Medio "Ramón Margalef," Universidad de Alicante, 03690 Alicante, Spain, and also with the Departamento de Ecología, Universidad de Alicante, 03690 Alicante, Spain (e-mail: ft.maestre@gmail.com).

This article has supplementary downloadable material available at https://doi.org/10.1109/TGRS.2021.3113594, provided by the authors.

Digital Object Identifier 10.1109/TGRS.2021.3113594

I. Introduction

DRYLANDS, defined as areas with an aridity index (i.e., the ratio of mean annual precipitation to mean annual potential evapotranspiration) below 0.65 [1], represent ∼41% of the earth's land surface [2] and host ∼38% of the world's population [3]. These areas are highly vulnerable to climate change [4] and land degradation driven by human activities [2]. Ecosystem attributes, such as vegetation structure and soil nutrient contents, and processes, such as productivity and nutrient cycling, are commonly used and/or suggested to assess ecosystem health [5], [6] and identify the onset of desertification [7]–[9], which is one of the main environmental issues facing drylands worldwide [2], [10]–[12]. Therefore, the monitoring of these ecosystem features is commonly highlighted as a key approach to combat land degradation and desertification [2], [13].

Assessing ecosystem structure and functioning using ground-based soil [14] and vegetation [5], [15] indicators is usually time-consuming, labor-intensive, expensive, and difficult to implement across large regions [14], [16], [17]. This is particularly true in remote areas with difficult access or where it is unsafe to conduct fieldwork, as is the case of many dryland regions worldwide. Remote sensing is almost the only realistic way to collect data and develop proxies of ecosystem structure and functioning safely and cost-effectively across large regions [18], [19]. Remotely sensed vegetation indices (VIs), such as the normalized difference vegetation index (NDVI), have been used to monitor ecosystem functioning in drylands worldwide at multiple scales, from local [20]–[22] to regional [23]–[25] and global [26], [27] scales. Remotely sensed albedo (defined as the ratio of upwelling to downwelling radiative flux at the surface) is another commonly used indicator to monitor dryland degradation due to its close relationship with land surface changes [28]–[32]. Zhao *et al.* [26] found significant correlations between broadband albedo metrics and ecosystem multifunctionality (i.e., a proxy of the capacity of the ecosystem to provide multiple functions simultaneously) in global drylands. Narrowband albedo/reflectance metrics have also been used to predict and map soil organic carbon (a proxy of soil fertility that is a critical determinant of multiple ecosystem processes and services [33], [34]) based on spaceborne, airborne platforms, and unmanned aerial systems [35]–[37].

Emerging evidence suggests that abrupt changes in multiple functional and structural ecosystem attributes, including albedo, vegetation cover, productivity, and soil organic carbon and nitrogen, occur when aridity increases beyond particular thresholds [39]. However, it is unknown whether these thresholds exist in the relationships between remotely sensed indicators (RSIs) and ground-based indicators of ecosystem functioning, which underpins the statistical models (e.g., regression models, random forests, and support vector machine) commonly used to estimate ecosystem functioning at large spatial scales by employing RSI as predictors [23], [35]–[38]. Addressing this issue is important because if such thresholds exist; they should be incorporated into these relationships to make them more robust and increase their predictive ability across the wide aridity gradients found across drylands worldwide. Here, we evaluated how the relationships between nutrient cycling index (NCI; a proxy of ecosystem functioning) measured *in situ* and RSI (albedo and NDVI) change along a wide aridity gradient in Patagonia (Argentina). As thresholds have been found when evaluating the relationships between aridity and both RSI and proxies of ecosystem functioning measured *in situ* in drylands [39], we hypothesized that aridity thresholds exist in the relationships between NCI and RSI.

II. Materials and Methods

A. Study Area

We used, for this study, 235 field sites from MARAS (Spanish acronym for "Environmental Monitoring for Arid and Semi-Arid Regions" [17]), a network of field sites located across Patagonia, in southern Argentina (see Fig. 1). All these sites were surveyed twice during the 2008–2018 period. Field data were gathered from 50 × 30 m plots with <10% slope in homogeneous areas of natural vegetation (see [17] for full details of the field survey). Aridisols and Entisols, with loam-sandy and sandy textures [40], are dominant soils across the study area. Vegetation is dominated by grasslands, shrub-grass steppes, shrublands, and semideserts. Average annual precipitation and temperature across the surveyed sites vary from 100 to 750 mm and from −4.5 °C to 16 °C, respectively [17].

B. Ecosystem Functions and Vegetation Cover Measured in the Field

Nutrient cycling is an essential ecosystem function that supports key ecosystem services, including food and fuel production and climate regulation [3]. To quantify it, we obtained from all the field sites studied the NCI of Tongway and Hindley [5], which is an indicator of how efficiently organic matter is cycled back into the soil. Studies conducted both in Patagonia [41] and in other drylands from Australia [42], Spain [43], [44], South Africa [45], Iran [46], Morocco [47], and Tunisia [48] have found strong correlations between NCI and quantitative measurements of soil variables related to microbial activity and nutrient cycling, such as soil pH, total soil N and P, soil organic carbon, soil respiration, and phosphatase and b-glucosidase activities.

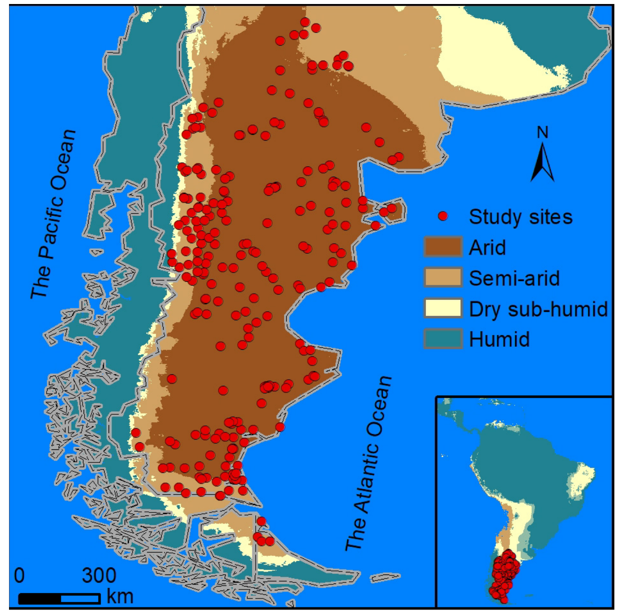

Fig. 1. Distribution of the 235 field sites used in this study across Argentinean Patagonia.

At each plot, multiple indicators related to vegetation and soil conditions were measured in three 50-m-long transects oriented in the main resource flow direction (see [17] and [49]). Perennial vegetation cover along the transect was quantified using the point-intercept method [50]. The NCI was assessed at each plot by evaluating multiple soil surface features (total soil cover, aerial canopy cover of perennial grasses and shrubs, litter cover, origin and degree of decomposition, and soil surface roughness) as described by Oliva *et al.* [4], [17]. See [17] and [49] for additional details on the field sampling and [5] for additional details on the process of calculating NCI. Fieldwork was conducted during the growing season (September to February) twice: between the years 2008 and 2013 (first evaluation) and between 2014 and 2018 (second evaluation). The mean time difference between both evaluations at each site was 6.0 + 1.4 years.

C. Remotely Sensed Indicators Used

We quantified the white-sky albedo (WSA) and NDVI of all the field sites surveyed using remote sensing. WSA is defined as the fraction of incident radiation that is reflected by a surface obtained from the condition that only isotropic illumination exists [51]. It is determined purely by the land surface reflective properties and is independent of atmospheric conditions and solar zenith angle [52].

We derived WSA at seven narrow bands (hereafter referred to as B1_WSA, B2_WSA, …, B7_WSA, respectively) from MODIS MCD43A3 BRDF/Albedo Model Parameters Product (Collection 6 [52]); the spectral range for each WSA band (B1-B7) is the following wavelength in nm: B1 = 620–670, B2 = 841–876, B3 = 459–479, B4 = 545–565, B5 = 1230–1250, B6 = 1628–1652, and B7 = 2105–2155. The algorithm used for the retrieval of this product was the RossThick-LiSparse-Reciprocal (Ross-Li) Bidirectional Reflectance Distribution Function (BRDF) model [53], [54], which uses multiple cloud-cleared land surface reflectance data over 16 days as inputs [52]. The product provides seven narrowband WSA bands daily since the year 2000 with a resolution of 500 m [52]. We used the Google Earth Engine (GEE) cloud computing platform for extracting WSA values on the field sampling date for the 235 sites. WSA quality/reliability is indicated by flags of 0 (Processed, good quality), 1 (Processed, see other QA), and 255 (Fill Value). To avoid using data with poor quality, WSA with flags of 1 and 255 were replaced by that with a flag of 0 around the field survey dates ($\sim$11% of the albedo data used were replaced). Finally, we calculated NDVI as [55]

$$\mathrm{NDVI} = \frac{\mathrm{B2\_WSA} - \mathrm{B1\_WSA}}{\mathrm{B2\_WSA} + \mathrm{B1\_WSA}} \tag{1}$$

where B1_WSA and B2_WSA are WSAs at red and near-infrared bands of MODIS, respectively.

D. Assessing Aridity Conditions

We used the aridity index, defined as precipitation/potential evapotranspiration [1], to depict the degree of dryness the drylands evaluated. We obtained aridity data for all the surveyed sites from the Global Aridity Index and Potential Evapotranspiration Climate Database v2 [56], which is modeled from the WorldClim global climate data [57]. This database provides averaged aridity index values for the period 1970–2000 with a spatial resolution of 30 arc-seconds ($\sim$1 km at the equator) and is widely used in ecological studies [39], [58]–[60]. To facilitate the interpretation of our results, 1-AI was used to characterize the degree of aridity of the studied sites [39].

E. Ecosystem Functions and Vegetation Cover Measured in the Field

To explore whether the RSI–NCI relationship responds to aridity in a nonlinear way, we first fit the responses of both RSI and NCI to aridity using four linear and nonlinear models (linear, quadratic polynomial, logistic, and logarithm) according to the following equations:

$$f(X) = aX + b \tag{2}$$

$$f(X) = aX^2 + bX + c \tag{3}$$

$$f(X) = \frac{d}{1 + ce^{-aX+b}} \tag{4}$$

$$f(X) = a \times \ln(X) + b \tag{5}$$

where $f(X)$ is the dependent variable, i.e., NCI, X is the independent variable, i.e., albedos/NDVI, and *a, b, c,* and *d* are parameters to be fit. This step is necessary because nonlinear responses of RSI and NCI to aridity can indicate that aridity thresholds may exit in RSI and NCI and their relationships.

Then, we explored how the RSI–NCI relationship changes in response to aridity across our study area. For doing so, all the four models were fit to the RSI–NCI relationship using a moving window with a size of 50 sites along the aridity gradient. We performed 200 bootstrap samplings for each fitting and identified the best model using three hierarchical rules [61].

1) The parameter a in (2)–(5) needs to be significant ($P \leq 0.05$) in the four models.
2) For those models where a was significant, we selected the best models using the Akaike information criteria (AICs 62]), where a lower AIC value represents a better model.
3) There are no differences in performance between two or more models if they showed a difference in AIC values lower than 2 [62]. When this happened, we selected the simplest model as the best by the priority: linear > logarithm > quadratic > logistic.

We found that the linear model was the best model fitting the RSI–NCI relationship in the moving windows along aridity evaluated (see Section III-B). Therefore, we used the Spearman correlation coefficient as the metric to quantify changes in the RSI–NCI relationship across the range of aridity conditions found in our study area. We selected the Spearman correlation because not all the variables were normally distributed in our study. All the analyses presented in this section were done by using MATLAB 9.1.0 (The Mathworks, Natick, MA, USA).

F. Detecting Thresholds in the Response of RSI–NCI Relationship to Aridity

A visual examination of the data showed that the Spearman correlation coefficient between RSI and NCI responded apparently in a nonlinear way to changes in aridity (see Section III-C). Thus, we further used segmented regression to explore the presence of aridity thresholds in the NCI–RSI relationship. Segmented regression can depict the relationships between response and explanatory variables by two or more straight lines connected at unknown values, which are usually referred to as threshold points [63]. The location of the threshold point is determined by the least-squares method [64], which can minimize the total error from each segment. We fit the response of Spearman correlation coefficients between RSI and NCI to aridity using a segmented regression with three thresholds. We set three thresholds because: 1) this is the number of thresholds revealed by Berdugo *et al.* [39] for global drylands and 2) the AIC obtained from fitting a model with three thresholds had a smaller value than the AIC values of models with one/two thresholds (see Table S1 in the Supplementary Material). We performed 200 bootstrap samplings before fitting the data using the segmented regression, and the median of 200 bootstrapped thresholds was employed as the final threshold. The segmented package from R software [63] was used to implement the segmented regressions.

TABLE I

AIC OF THE MODELS FITTING THE RESPONSES OF RSIS AND NCI TO ARIDITY. B1_WSA, ..., B7_WSA ARE WSAS AT BAND1, ..., BAND7 OF MODIS, RESPECTIVELY. THE VALUES WITH GRAY BACKGROUND REPRESENT THE MODEL FIT WAS NOT SIGNIFICANT, WHICH WILL NOT BE USED FOR COMPARISON. VALUES IN BOLD INDICATE THE BEST MODEL FIT IN EACH CASE

Variables	Akaike Information Criterion							
	First sampling date (2008-2013)				Second sampling date (2014-2018)			
	Linear	Quadratic	Logistic	Logarithm	Linear	Quadratic	Logistic	Logarithm
B1_WSA	-1034	**-1042**	-1037	-1032	-1014	**-1025**	-1015	-1013
B2_WSA	**-953**	-954	-953	-952	**-912**	-913	-912	-912
B3_WSA	-1314	**-1321**	-1315	-1312	-1309	**-1319**	-1310	-1307
B4_WSA	-1175	**-1181**	-1175	-1174	-1161	**-1168**	-1161	-1160
B5_WSA	-884	**-886**	-886	-883	-823	**-828**	-826	-823
B6_WSA	-849	-852	-852	-849	-855	-855	-854	-855
B7_WSA	**-933**	-933	-933	-933	-915	**-921**	-915	-915
NDVI	-542	**-559**	-559	-536	-461	**-480**	-474	-458
NCI	1644	**1641**	1642	1646	1748	**1740**	1742	1750

III. RESULTS

A. Responses of RSI and NCI to Aridity

According to the AIC (see Table I) and the significance of coefficient *a* (see Table S2 in the Supplementary Material) of the models, the quadratic polynomial model was best for fitting the response of B1_WSA, B3_WSA, B4_WSA, B5_WSA, NDVI, and NCI to aridity during the first sampling date (see Table I and Fig. 2). The linear model, however, was a better fit to the relationships between B2_WSA and B7_WSA and aridity (see Table I and Fig 2). None of the models tested significantly fit the response of B6_WSA to aridity (see Table I). Similar results were obtained when analyzing data from the second sampling date, except that the best model was quadratic polynomial for the response of B7_WSA to aridity (see Table I and Table S2 and Fig. S1 in the Supplementary Material).

B. Characteristics of the RSI–NCI Relationship

For the models fitting the relationships between visible albedos (BI_WSA, B3_WSA, and B4_WSA) and NCI, the coefficient *a* in the linear and logarithm models was significant ($p < 0.5$) at most aridity levels except around 0.8 [see Fig. 3(a)–(f)]. The *a* values obtained from quadratic polynomial and logistic models exhibited significance at small portions of the aridity range evaluated. For the models fitting the relationship between NDVI and NCI, *a* in the linear and logarithm model was significant at almost all aridity levels for both sampling dates. These results indicated that the linear and logarithmic models were better than quadratic polynomial and logistic models to fit the RSI–NCI relationships in the moving window along the aridity gradient evaluated. We further compared the AIC values obtained from linear and logarithmic models in each moving window. The absolute value difference was lower than 2 (see Fig. S3 in the Supplementary Material), which indicated that the performance of the two models was similar. Considering that the linear model is simpler and easier to interpret, we selected this model as a suitable one to describe RSI–NCI relationships along the aridity gradient evaluated. For the coefficient *a* in the models fitting the relationships between infrared albedos (B2_WSA, B5_WSA, B6_WSA, and B7_WSA) and NCI, they were all not significant at most aridity levels (see Fig. S2 in the Supplementary Material). Therefore, we excluded the infrared albedos in further analyses of our data.

C. Aridity Thresholds Identified in the Relationships Between RSI and NCI

The response of the linear relationships between RSI and NCI, quantified using the Spearman correlation coefficient, to changes in aridity was apparently nonlinear at both sampling dates (see Fig. 4). The use of segmented regression revealed the presence of three aridity thresholds in the relationships between RSI and NCI (see Fig. 4). The slopes and intercepts both showed significant differences before and after each threshold (p-value <0.01 using a Mann–Whitney U test). The first threshold exhibited a wide range, as it was found at aridity values from 0.44 to 0.60; the second and third thresholds were found around aridity values of 0.69 and 0.82, respectively (see Fig. 4). The relationships between NCI and the visible albedos were not significant around the third aridity threshold (i.e., 0.82).

IV. DISCUSSION

A. Models Fitting the RSI–NCI Relationships

Our results showed that both RSI (B1_WSA, B3_WSA, B4_WSA, B5_WSA, and NDVI) and NCI showed nonlinear responses to aridity at both sampling dates. This is consistent with a recent report showing that multiple functional and structural ecosystem attributes exhibited nonlinear responses to aridity across global drylands [39]. The nonlinear responses indicated that aridity thresholds may exist in B1_WSA, B3_WSA, B4_WSA, B5_WSA, NDVI, NCI, and, most importantly, in their relationships, a response not reported before.

We also found that the linear model was the best model fitting the RSI–NCI relationship at most aridity levels. This agrees with results from recent research reporting that albedo metrics derived from MODIS had a significant linear relationship with multifunctionality indices related to carbon, nitrogen,

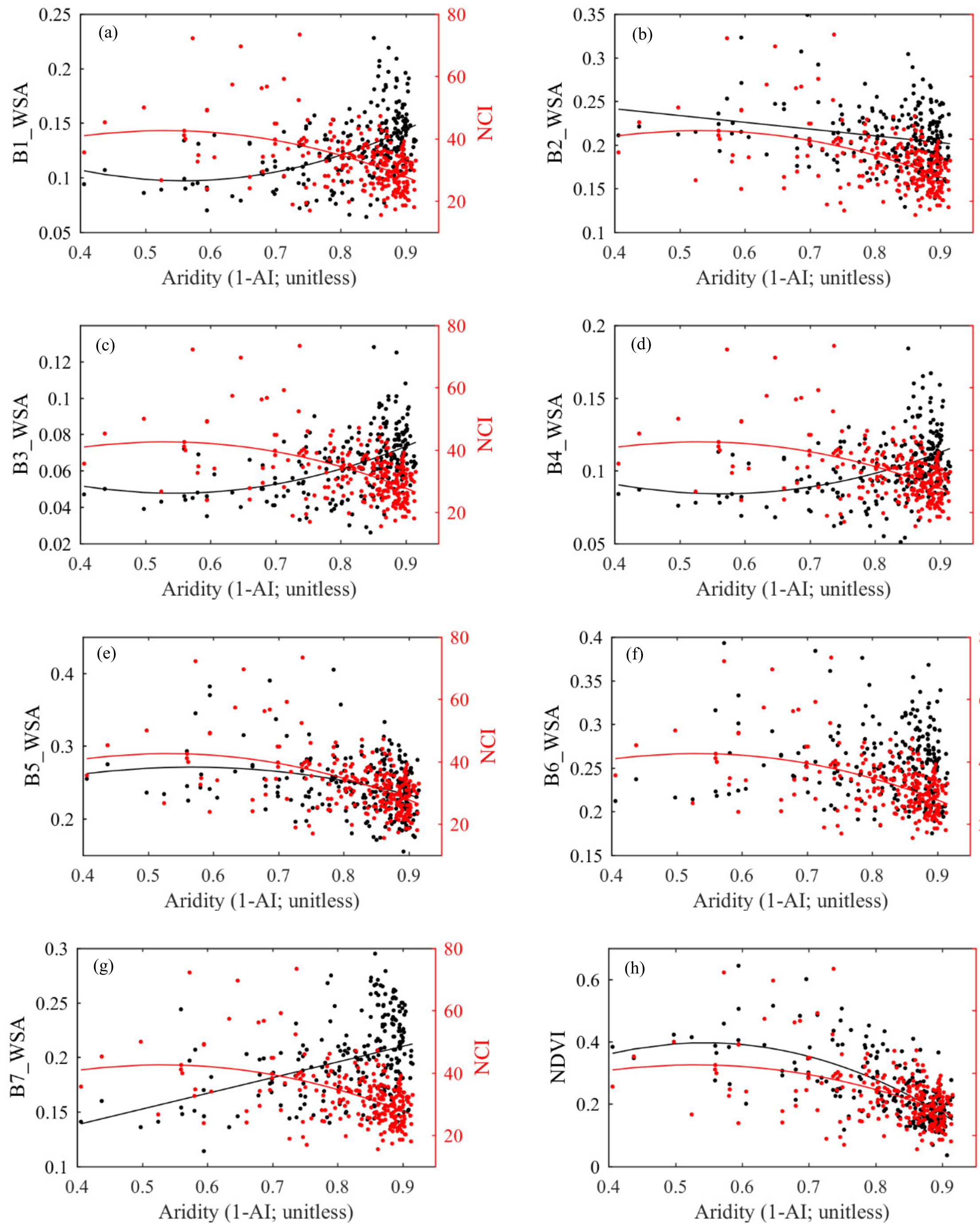

Fig. 2. Responses of RSIs and NCI to aridity using data from the first sampling date (2008–2013). Colored solid lines represent the fit by the best model. The responses of B1_WSA, B3_WSA, B4_WSA, B5_WSA, NDVI, and NCI to aridity are fit by the quadratic polynomial model, and those for B2_WSA and B7_WSA are fit by the linear model. B1_WSA, …, B7_WSA are WSAs at band1, …, band7 of MODIS, respectively. See Fig. S1 in the Supplementary Material for results from the second sampling date (2014–2018).

and phosphorus cycling in global drylands [26]. NDVI has been commonly used as the surrogation of the ecosystem functions due to its close relationship with above-ground net primary productivity [65]–[67]. In addition, both visible albedos and NDVI have been found to be correlated with vegetation cover [21], which has been reported to be a key driver of ecosystem function across Patagonian drylands [68]. Therefore, it is not surprising that linear models properly fit the relationships of visible albedos and NDVI with NCI at most of the aridity levels evaluated. However, the models fitting the relationships between infrared albedos and NCI were not significant at most aridity levels (see Fig. S2 in the Supplementary Material). This result also agrees with previous findings showing nonsignificant correlations between infrared albedo and surrogates of carbon and nutrient cycling across global drylands [26].

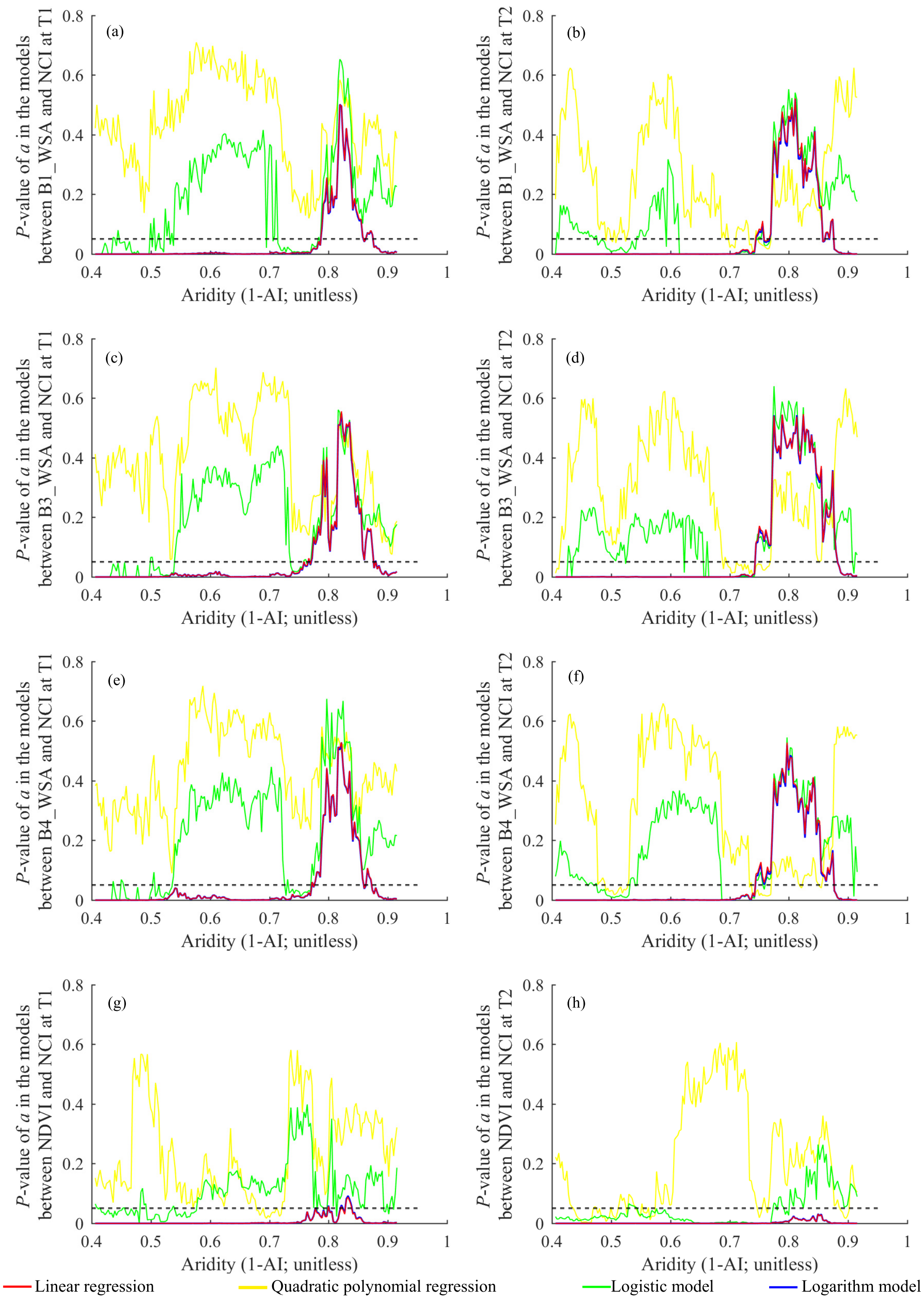

Fig. 3. p-values of the parameter a in the models fit between RSIs and NCI along the aridity gradient evaluated. The linear (red line) and logarithm (blue line) models almost overlapped because they had a very similar performance. The black dash lines indicate a p-value of 0.05. T1 and T2 represent data from the first and second sampling dates, respectively. B1_WSA, B3_WSA, and B4_WSA are WSAs at band1, band3, and band4 of MODIS, respectively.

B. Aridity Thresholds Should Be Considered When Employing Remotely Sensed Indicators to Evaluate Ecosystem Functions

It has been reported that aridity thresholds exist in various ecosystem processes in drylands [39], [69], [70]. Our results demonstrated that three aridity thresholds existed in the relationships (quantified by the Spearman correlation coefficients) between RSI (e.g., visible albedo and NDVI) and NCI. The first aridity thresholds exhibited a wide range from 0.44 to around 0.60, which covers the threshold value of 0.54 identified by Berdugo *et al.* [39] for multiple vegetation attributes (photosynthesis and leaf nutrient content) across global drylands. The second and third thresholds were around the aridity

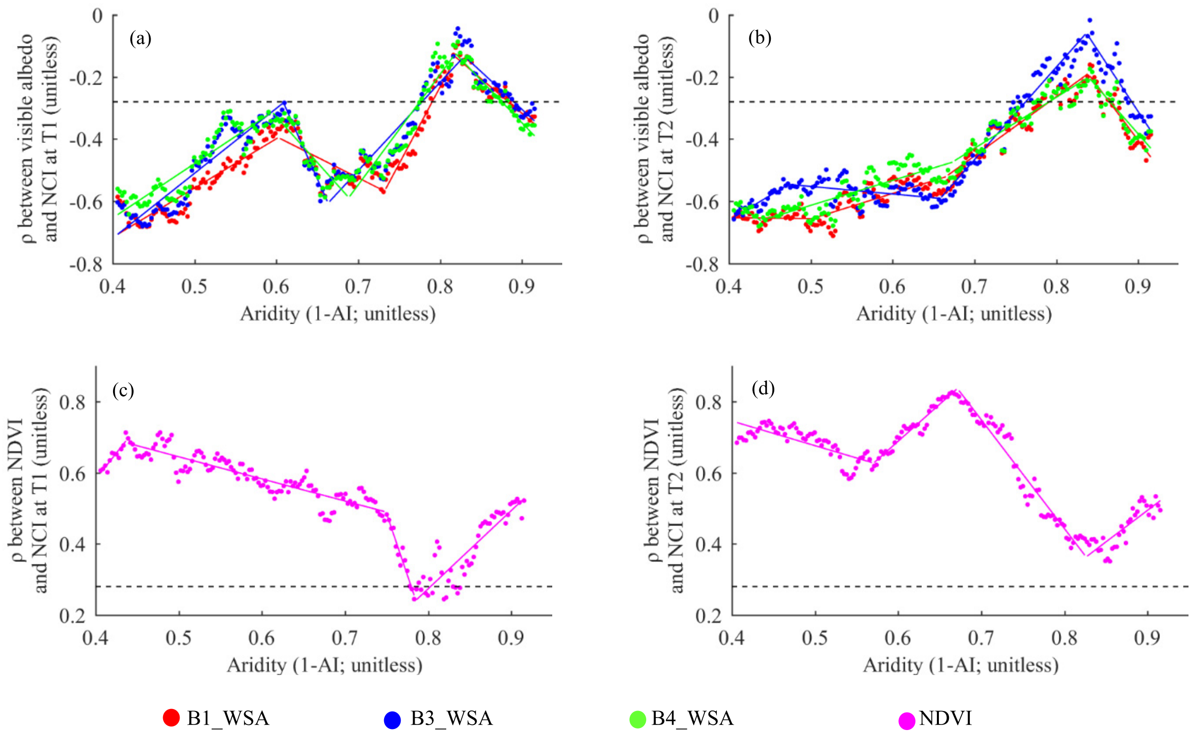

Fig. 4. Aridity thresholds identified in the correlations between RSIs and NCI. Colored solid lines represent the linear fits at both sides of each threshold. The black dashed lines indicate the significance level of correlation coefficients ($p < 0.05$). T1 and T2 represent data from the first and second sampling dates, respectively. B1_WSA, B3_WSA, and B4_WSA are WSAs at band1, band3, and band4 of MODIS, respectively.

of 0.69 and 0.82, respectively. These thresholds are consistent with the results of other studies exploring the response of ecosystem properties to aridity in drylands. For example, soil fertility, plant nitrogen content, and biotic interactions show sharp declines at aridity values around 0.7 [39]; plant cover, albedo, vegetation spatial patterns, nitrogen turnover rates, and mechanisms driving the structure of plant communities all show sharp changes at aridity values around 0.8 [33], [39], [69].

The presence of these three aridity thresholds indicates that the RSI–NCI relationships change drastically along the aridity gradient observed in Patagonian drylands. Therefore, we suggest that these nonlinearities determined by aridity should be incorporated when evaluating the relationships between RSI and surrogates of ecosystem functioning measured *in situ*. Our results show that both linear and nonlinear relationships between NCI and the albedo metrics used were not significant around aridity value of 0.82. This indicates empirical models (e.g., random forests models and partial least-squares regression) employing only albedos/reflectance as predictors, such as those reported by Vågen *et al.* [35], Vaudour *et al.* [71], and Castaldi *et al.* [72], should be revised in regions with similar aridity level.

The mean time difference between the twice sampling dates was about six years. Both RSI and NCI had high temporal relative changes in some filed sites (see Fig. S4 in the Supplementary Material). However, the three aridity thresholds, particularly the second and third ones, exiting in RSI–NCI relationship were similar in the two dates. This further indicates that the aridity thresholds that we found from spatial gradients were maintained during the time frame evaluated, something that adds robustness to the results observed.

V. Conclusion

To explore whether aridity thresholds exist in the relationships between ecosystem functioning and RSI, we linked NDVI and seven narrowband albedos derived from MODIS to NCI using field data from 235 sites located in Patagonia, Argentina, covering a wide aridity gradient. We found both RSI and NCI responded nonlinearly to aridity. We further employed four linear and nonlinear models to fit the RSI–NCI relationships in a moving window along the aridity gradient evaluated and found that the linear model was optimal at most aridity levels. By using segmented regressions, we finally identified three aridity thresholds existing in the RSI–NCI relationships, which indicates that these relationships change drastically along the aridity gradient evaluated. Particularly, relationships between NCI and albedos were all not significant around the threshold of 0.82, which implies that empirical models employing only albedos/reflectance as inputs could be disputed in regions with high aridity. It is important to note that our results were maintained regardless of the sampling date considered. Our findings indicate that aridity thresholds should be considered when assessing ecosystem functioning using RSIs and are useful for improving the effectiveness of their use to monitor and predict changes in ecosystem functioning across large environmental gradients, such as those found across Patagonia.

ACKNOWLEDGMENT

The authors would like to thank Marina Dacal and Sergio Asensio for the discussion about the metrics used to select the best model.

REFERENCES

[1] N. Middleton and D. S. G. Thomas, Eds., *UNEP, World Atlas of Desertification*. London, U.Edward Arnold Press, 1992, p. 2.
[2] M. Cherlet, C. Hutchinson, J. Reynolds, J. Hill, S. Sommer, and G. Von Maltitz, *World Atlas of Desertification: Rethinking Land Degradation and Sustainable Land Management*. Luxembourgish, French: Publications Office of the European Union, 2018 p. 2.
[3] *Millennium Ecosystem Assessment, Ecosystems and Human Well-Being: Desertification Synthesis*, World Resources Institute, Washington, DC, USA, 2005, p. 2.
[4] J. Huang, H. Yu, X. Guan, G. Wang, and R. Guo, "Accelerated dryland expansion under climate change," *Nature Climate Change*, vol. 6, no. 2, pp. 166–171, Feb. 2016.
[5] D. J. Tongway and N. L. Hindley, "Landscape function analysis: Procedures for monitoring and assessing landscapes-with special reference to minesites and rangelands," in *Sustainable Ecosystems, Commonwealth Scientific and Industrial Research Organisation*. Canberra, ACT, Australia: CSIRO Sustainable Ecosystems, 2004, pp. 97–112.
[6] J. E. Herrick, B. T. Bestelmeyer, Archer, S. Tugel, and J. R. Brown, "An integrated framework for science-based arid land management," *J. Arid Environ*, vol. 65, no. 2, pp. 319–335, 2006.
[7] S. K?fi *et al.*, "Spatial vegetation patterns and imminent desertification in Mediterranean arid ecosystems," *Nature*, vol. 449, no. 7159, pp. 213–217, 2007.
[8] F. T. Maestre and A. Escudero, "Is the patch size distribution of vegetation a suitable indicator of desertification processes?" *Ecology*, vol. 90, no. 7, pp. 1729–1735, Jul. 2009.
[9] M. Berdugo, S. Kéfi, S. Soliveres, and F. T. Maestre, "Plant spatial patterns identify alternative ecosystem multifunctionality states in global drylands," *Nature Ecol. Evol.*, vol. 1, no. 2, pp. 1–10, Feb. 2017.
[10] S. R. Verón, L. J. Blanco, M. A. Texeira, J. G. N. Irisarri, and J. M. Paruelo, "Desertification and ecosystem services supply: The case of the arid Chaco of South America," *J. Arid Environ.*, vol. 159, pp. 66–74, Dec. 2018.
[11] H. Weissmann, R. Kent, Y. Michael, and N. M. Shnerb, "Empirical analysis of vegetation dynamics and the possibility of a catastrophic desertification transition," *PLoS ONE*, vol. 12, no. 12, Dec. 2017, Art. no. e0189058.
[12] J. Huang, G. Zhang, Y. Zhang, X. Guan, Y. Wei, and R. Guo, "Global desertification vulnerability to climate change and human activities," *Land Degrad. Dev.*, vol. 31, no. 10, pp. 1380–1391, 2020.
[13] J. F. Reynolds *et al.*, "Global desertification: Building a science for dryland development," *Science*, vol. 316, pp. 847–851, May 2007.
[14] F. T. Maestre *et al.*, "Plant species richness and ecosystem multifunctionality in global drylands," *Science*, vol. 335, no. 6065, pp. 214–218, 2012.
[15] D. J. Tongway, *Rangeland Soil Condition Assessment Manual*. Canberra, ACT, Australia: CSIRO Division of Wildlife and Ecology, 1994, pp. 9–27.
[16] R. Ochoa-Hues *et al.*, "Soil fungal abundance and plant functional traits drive fertile island formation in global drylands," *J. Ecol.*, vol. 106, no. 1, pp. 53–242, 2017.
[17] G. Oliva *et al.*, "The MARAS dataset, vegetation and soil characteristics of dryland rangelands across Patagonia," *Sci. Data*, vol. 7, no. 1, pp. 1–14, Dec. 2020.
[18] N. Pettorelli *et al.*, "Satellite remote sensing of ecosystem functions: Opportunities, challenges and way forward," *Remote Sens. Ecol. Conservation*, vol. 4, no. 2, pp. 71–93, 2018.
[19] J. Cabello *et al.*, "The ecosystem functioning dimension in conservation: Insights from remote sensing," *Biodiversity Conservation*, vol. 21, no. 13, pp. 3287–3305, Dec. 2012.
[20] M. García-Gómez and F. T. Maestre, "Remote sensing data predict indicators of soil functioning in semi-arid steppes, central Spain," *Ecol. Indic.*, vol. 11, no. 5, pp. 1476–1481, 2011.
[21] T. B. Poitras, M. L. Villarreal, E. K. Waller, T. W. Nauman, M. E. Miller, and M. C. Duniway, "Identifying optimal remotely-sensed variables for ecosystem monitoring in Colorado plateau drylands," *J. Arid Environ.*, vol. 153, pp. 76–87, Jun. 2018.
[22] C. Abel, S. Horion, T. Tagesson, M. Brandt, and R. Fensholt, "Towards improved remote sensing based monitoring of dryland ecosystem functioning using sequential linear regression slopes (SeRGS)," *Remote Sens. Environ.*, vol. 224, pp. 317–332, 2019.
[23] J. J. Gaitán *et al.*, "Evaluating the performance of multiple remote sensing indices to predict the spatial variability of ecosystem structure and functioning in Patagonian steppes," *Ecol. Indicators*, vol. 34, pp. 181–191, Nov. 2013.
[24] T. Sternberg, R. Tsolmon, N. Middleton, and D. Thomas, "Tracking desertification on the Mongolian steppe through NDVI and field-survey data," *Int. J. Digit. Earth*, vol. 4, no. 1, pp. 50–64, Jan. 2011.
[25] T. P. Higginbottom and E. Symeonakis, "Identifying ecosystem function shifts in Africa using breakpoint analysis of long-term NDVI and RUE data," *Remote Sens.*, vol. 12, no. 11, p. 1894, Jun. 2020.
[26] Y. Zhao, X. Wang, C. J. Novillo, P. Arrogante-Funes, R. Vázquez-Jiménez, and F. T. Maestre, "Albedo estimated from remote sensing correlates with ecosystem multifunctionality in global drylands," *J. Arid Environ.*, vol. 157, pp. 116–123, Oct. 2018.
[27] R. Fensholt *et al.*, "Global-scale mapping of changes in ecosystem functioning from earth observation-based trends in total and recurrent vegetation," *Global Ecol. Biogeogr.*, vol. 24, no. 9, pp. 1003–1017, 2015.
[28] A. Karnieli, Z. Qin, B. Wu, N. Panov, and F. Yan, "Spatio-temporal dynamics of land-use and land-cover in the Mu Us sandy land, China, using the change vector analysis technique," *Remote Sens.*, vol. 6, no. 10, pp. 9316–9339, Sep. 2014.
[29] C. J. Robinove, P. S. Chavez, D. Gehring, and R. Holmgren, "Arid land monitoring using landsat albedo difference images," *Remote Sens. Environ.*, vol. 11, pp. 133–156, Jan. 1981.
[30] M. Lamchin *et al.*, "Assessment of land cover change and desertification using remote sensing technology in a local region of Mongolia," *Adv. Space Res.*, vol. 57, no. 1, pp. 64–77, Jan. 2016.
[31] G. Tripathy, T. Ghosh, and S. Shah, "Monitoring of desertification process in Karnataka state of India using multi-temporal remote sensing and ancillary information using GIS," *Int. J. Remote Sens.*, vol. 17, no. 12, pp. 2243–2257, 1996.
[32] Y. Zhao *et al.*, "Remotely sensed albedo allows the identification of two ecosystem states along aridity gradients in Africa," *Land Degradation Develop.*, vol. 30, no. 12, pp. 1502–1515, Jul. 2019.
[33] P. Pereira, I. Bogunovic, M. Muñoz-Rojas, and E. C. Brevik, "Soil ecosystem services, sustainability, valuation and management," *Current Opinion Environ. Sci. Health*, vol. 5, pp. 7–13, Oct. 2018.
[34] C. Plaza, G. Gascó, A. M. Méndez, C. Zaccone, and F. T. Maestre, "Soil organic matter in dryland ecosystems," in *The Future of Soil Carbon*. Cambridge, MA, USA: Academic, 2018, pp. 39–70.
[35] T.-G. Vågen, L. A. Winowiecki, J. E. Tondoh, L. T. Desta, and T. Gumbricht, "Mapping of soil properties and land degradation risk in Africa using MODIS reflectance," *Geoderma*, vol. 263, pp. 216–225, Feb. 2016.
[36] A. Gholizadeh, D. Žižala, M. Saberioon, and L. Boruvka, "Soil organic carbon and texture retrieving and mapping using proximal, airborne and Sentinel-2 spectral imaging," *Remote Sens. Environ.*, vol. 218, pp. 89–103, Dec. 2018.
[37] T. Angelopoulou, N. Tziolas, A. Balafoutis, G. Zalidis, and D. Bochtis, "Remote sensing techniques for soil organic carbon estimation: A review," *Remote Sens.*, vol. 11, no. 6, p. 676, Mar. 2019.
[38] H. Dashti *et al.*, "Empirical methods for remote sensing of nitrogen in drylands may lead to unreliable interpretation of ecosystem function," *IEEE Trans. Geosci. Remote Sens.*, vol. 57, no. 6, pp. 3993–4004, Jun. 2019.
[39] M. Berdugo *et al.*, "Global ecosystem thresholds driven by aridity," *Science*, vol. 367, no. 6479, pp. 787–790, Feb. 2020.
[40] H. F. del Valle, "Patagonian soils: A regional synthesis," *Ecología Austral*, vol. 8, no. 2, pp. 103–123, 1998.
[41] J. J. Gaitán *et al.*, "Aridity and overgrazing have convergent effects on ecosystem structure and functioning in Patagonian rangelands," *Land Degrad. Dev.*, vol. 29, no. 2, pp. 210–218, 2018.
[42] A. M. Holm, L. T. Bennett, W. A. Loneragan, and M. A. Adams, "Relationships between empirical and nominal indices of landscape function in the arid shrubland of western Australia," *J. Arid Environ.*, vol. 50, no. 1, pp. 1–21, Jan. 2002.
[43] F. T. Maestre and M. D. Puche, "Indices based on surface indicators predict soil functioning in Mediterranean semi-arid steppes," *Appl. Soil Ecol.*, vol. 41, no. 3, pp. 342–350, 2009.
[44] Á. G. Mayor and S. Bautista, "Multi-scale evaluation of soil functional indicators for the assessment of water and soil retention in Mediterranean semiarid landscapes," *Ecol. Indicators*, vol. 20, pp. 332–336, Sep. 2012.

[45] D. Parker, R. Bernard, and J. Adendorff, “Do elephants influence the organisation and function of a South African grassland,” *Rangeland J.*, vol. 31, no. 4, pp. 395–403, 2009.

[46] S. A. Rezaei, H. Arzani, and D. Tongway, “Assessing rangeland capability in Iran using landscape function indices based on soil surface attributes,” *J. Arid Environ.*, vol. 65, no. 3, pp. 460–473, May 2006.

[47] M. Derak *et al.*, “Caractérisation du fonctionnement Des.steppes d’Alfa marocaines par la méthode de l’analyse fonctionnelle du paysage,” *Ecologia mediterranea*, vol. 41, no. 2, pp. 61–72, 2015.

[48] S. Derbel, J. Cortina, and M. Chaieb, “Acacia salignaPlantation impact on soil surface properties and vascular plant species composition in central Tunisia,” *Arid Land Res. Manage.*, vol. 23, no. 1, pp. 28–46, Jan. 2009.

[49] G. Oliva *et al.*, *Manual Para la Instalaci on Y Lectura de Monitores MARAS*. New York, NY, USA: PNUD, Buenos Aires, Argentina, 2011.

[50] D. D. Müller-Dombois and H. Ellenberg, *Aims and Methods of Vegetation Ecology*. New York, NY, USA: Wiley, 1974, p. 547.

[51] W. Lucht, C. B. Schaaf, and A. H. Strahler, “An algorithm for the retrieval of albedo from space using semiempirical BRDF models,” *IEEE Trans. Geosci. Remote Sens.*, vol. 38, no. 2, pp. 977–998, Mar. 2000.

[52] C. Schaaf and Z. Wang, *MCD43A4: MODIS/Terra+ Aqua BRDF/Albedo Nadir BRDF Adjusted RefDaily L3 Global-500m V006*. Washington, DC, USA: NASA EOSDIS Land Processes DAAC, 2015.

[53] I. Ross, *The Radiation Regime and Architecture of Plant Stands*. Norwood, MA, USA: Artech House, 2012, pp. 324–334.

[54] X. Li and A. H. Strahler, “Geometric-optical bidirectional reflectance modeling of the discrete crown vegetation canopy: Effect of crown shape and mutual shadowing,” *IEEE Trans. Geosci. Remote Sens.*, vol. 30, no. 2, pp. 276–292, Mar. 1992.

[55] J. W. Rouse, “Monitoring vegetation systems in the great plains with ERTS,” in *Proc. 3rd ERTS Symp.*, Washington, DC, USA, 1973, pp. 309–317.

[56] A. Trabucco and R. J. Zomer, *Global Aridity Index and Potential Evapotranspiration (ET0) Climate Database V2*. Montpellier, France: CGIAR Consortium for Spatial Information, 2018.

[57] S. E. Fick and R. J. Hijmans, “WorldClim 2: New 1-km spatial resolution climate surfaces for global land areas,” *Int. J. Climatol.*, vol. 37, no. 12, pp. 4302–4315, Oct. 2017.

[58] M. Larter, S. Pfautsch, J. Domec, S. Trueba, N. Nagalingum, and S. Delzon, “Aridity drove the evolution of extreme embolism resistance and the radiation of conifer genus *Callitris*,” *New Phytologist*, vol. 215, no. 1, pp. 112–197, Jul. 2017.

[59] N. Herrmann *et al.*, “Hydrogen isotope fractionation of leaf wax *n*-alkanes in Southern African soils,” *Organic Geochem.*, vol. 109, pp. 1–13, Jul. 2017.

[60] I. J. Wright *et al.*, “Global climatic drivers of leaf size,” *Science*, vol. 357, no. 6354, pp. 917–921, Sep. 2017.

[61] M. Delgado-Baquerizo *et al.*, “Changes in belowground biodiversity during ecosystem development,” *Proc. Nat. Acad. Sci. USA*, vol. 116, no. 14, pp. 6891–6896, 2019.

[62] H. Akaike, “A new look at the statistical model identification,” *IEEE Trans. Autom. Control*, vol. AC-19, no. 6, pp. 716–723, Dec. 1974.

[63] V. Muggeo, “Segmented: An R package to fit regression models with broken-line relationships,” *R News*, vol. 8, no. 1, pp. 20–25, 2008.

[64] E. P. D. Mansard and E. R. Funke, “The measurement of incident and reflected spectra using a least squares method,” in *Proc. Coastal Eng.*, Mar. 1980, pp. 154–172.

[65] J. M. Paruelo, H. E. Epstein, W. K. Lauenroth, and I. C. Burke, “ANPP estimates from NDVI for the central grassland region of the United States,” *Ecology*, vol. 78, no. 3, pp. 953–958, Apr. 1997.

[66] H. J. Richardson, D. J. Hill, D. R. Denesiuk, and L. H. Fraser, “A comparison of geographic datasets and field measurements to model soil carbon using random forests and stepwise regressions (British Columbia, Canada),” *GISci. Remote Sens.*, vol. 54, no. 4, pp. 573–591, Jul. 2017.

[67] O. Odebiri, O. Mutanga, J. Odindi, K. Peerbhay, and S. Dovey, “Predicting soil organic carbon stocks under commercial forest plantations in KwaZulu-natal province, South Africa using remotely sensed data,” *GISci. Remote Sens.*, vol. 57, no. 4, pp. 450–463, May 2020.

[68] J. J. Gaitán *et al.*, “Vegetation structure is as important as climate for explaining ecosystem function across Patagonian rangelands,” *J. Ecol.*, vol. 102, no. 6, pp. 1419–1428, Nov. 2014.

[69] C. Wang *et al.*, “Aridity threshold in controlling ecosystem nitrogen cycling in arid and semi-arid grasslands,” *Nature Commun.*, vol. 5, no. 1, pp. 1–8, Dec. 2014.

[70] J. Hou *et al.*, “Aridity thresholds of soil microbial metabolic indices along a 3,200 km transect across arid and semi-arid regions in Northern China,” *PeerJ*, vol. 7, Apr. 2019, Art. no. e6712.

[71] E. Vaudour, C. Gomez, Y. Fouad, and P. Lagacherie, “Sentinel-2 image capacities to predict common topsoil properties of temperate and Mediterranean agroecosystems,” *Remote Sens. Environ.*, vol. 223, pp. 21–33, Mar. 2019.

[72] F. Castaldi *et al.*, “Evaluating the capability of the sentinel 2 data for soil organic carbon prediction in croplands,” *ISPRS J. Photogramm. Remote Sens.*, vol. 147, pp. 267–282, Jan. 2019.

Yanchuang Zhao received the Ph.D. degree in cartography and geography information systems from the Chinese Academy of Sciences, Beijing, China, in 2018.

He is currently a Researcher with the College of Information Science and Engineering, Henan University of Technology, Zhengzhou, China. His research focuses on linking remote sensing to ecological structure and function in drylands to advance new tools for dryland monitoring and management.

Emilio Guirado received the master’s degree in water and environment in arid zones and the Ph.D. degree in environmental sciences from the University of Almería, Almería, Spain, in 2013 and 2019, respectively.

He is currently a Post-Doctoral Researcher with the Multidisciplinary Institute for the Study of the Environment (IMEM), University of Alicante, Alicante, Spain, where he investigates ecosystem functioning and biodiversity with remote sensing and deep learning perspective.

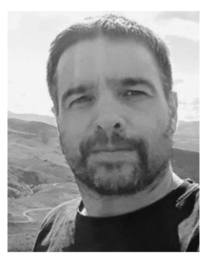

Juan J. Gaitán received the B.S. degree in agronomy from Luján University, Buenos Aires, Argentina, in 2002, and the M.Sc. degree in natural resources and the Ph.D. degree in agronomy from the Buenos Aires University, Buenos Aires, in 2009 and 2016, respectively.

He is currently a Research Scientist with the Soil Institute of National Institute of Agricultural Technology (INTA), an Adjunct Research Scientist with the National Research Council of Argentina (CONICET), and an Adjunct Professor with Luján University. His research interests include applied remote sensing to assess and monitor land degradation processes.

Fernando T. Maestre received the B.Sc. and Ph.D. degrees in biology from the University of Alicante, Alicante, Spain, in 1999 and 2002, respectively.

He is currently a Professor of ecology with Rey Juan Carlos University, Móstoles, Spain, and a Distinguished Researcher with the University of Alicante, where he leads the Dryland Ecology and Global Change Laboratory. His research focuses on understanding the ecology of global drylands and their responses to ongoing global environmental change and desertification.